Research Article | Vol. 25, No. 22 | 30 Oct 2017 | OPTICS EXPRESS 27172
Optics EXPRESS

Large-scale continuous-variable dual-rail cluster entangled state based on spatial mode comb

J. ZHANG,[1,2,4] J. J. WANG,[1,2] R. G. YANG,[1,2,4,*] K. LIU,[1,3,4] AND J. R. GAO[1,2,3,4]

[1] *State Key Laboratory of Quantum Optics and Quantum Optics Devices, Shanxi University, Taiyuan 030006, China*
[2] *College of Physics and Electronic Engineering, Shanxi University, Taiyuan 030006, China*
[3] *Institute of Opto-Electronics, Shanxi University, Taiyuan 030006, China*
[4] *Collaborative Innovation Center of Extreme Optics, Shanxi University, Taiyuan, 030006, China*
[*] *yrg@sxu.edu.cn*

Abstract: In recent continuous-variable (CV) multipartite entanglement researches, the number of fully inseparable light modes has been increased dramatically by the introduction of a multiplexing scheme in either the time domain or the frequency domain. In this paper, we propose a scheme that a large-scale ($\geq$ 20) CV dual-rail cluster entangled state is established based on a spatial mode comb in a self-imaging optical parametric oscillator, which is pumped by two spatial Laguerre-Gaussian modes with different polarization and identical frequency. A sufficient condition of full inseparability for a CV dual-rail cluster entangled state is used to evaluate the degree of quantum entanglement. It is shown that entanglement exists over a wide range of analyzing frequency and pump parameter. We have found a new scheme that uses the optical parametric cavity to generate a large-scale entanglement based on optical spatial mode comb. The presented system will be hopefully as a practical entangled source for quantum information.

OCIS codes: (270.0270) Quantum optics; (190.4410) Nonlinear optics, parametric processes; (270.2500) Fluctuations, relaxations, and noise.

References and links

1. M. Gu, C. Weedbrook, N. C. Menicucci, T. C. Ralph, and P. van Loock, "Quantum computing with continuous-variable clusters," Phys. Rev. A **79**, 062318 (2009).
2. J. Jing, J. Zhang, Y. Yan, F. Zhao, C. Xie, and K. Peng, "Experimental demonstration of tripartite entanglement and controlled dense coding for continuous variables," Phys. Rev. Lett. **90**, 167903 (2003).
3. T. J. Johnson, S. D. Bartlett, and B. C. Sanders, "Continuous-variable quantum teleportation of entanglement," Phys. Rev. A **66**, 042326 (2002).
4. O. Pfister, S. Feng, G. Jennings, R. Pooser, and D. Xie, "Multipartite continuous-variable entanglement from concurrent nonlinearities," Phys. Rev. A **70**, 020302(R) (2004).
5. R. Pooser and O. Pfister, "Observation of triply coincident nonlinearities in periodically poled $KTiOPO_4$," Opt. Lett. **19**, 2635–2637 (2005).
6. H. J. Briegel and R. Raussendorf, "Persistent Entanglement in Arrays of Interacting Particles," Phys. Rev. Lett. **86**, 910–913 (2001).
7. P. Dong, Z. Y. Xue, M. Yang, and Z. L. Cao, "Generation of cluster states," Phys. Rev. A **73**, 033818 (2006).
8. R. Shahrokhshahi and O. Pfister, "Large-scale multipartite entanglement in the quantum optical frequency comb of a depleted-pump optical parametric oscillator," Quantum Inf. Comput. **12**, 953–969 (2012).
9. R. Raussendorf, D. E. Browne, and H. J. Briegel, "Measurement-based quantum computation on cluster states," Phys. Rev. A **68**, 022312 (2003).
10. M. Pysher, Y. Miwa, R. Shahrokhshahi, R. Bloomer, and O. Pfister, "Parallel generation of quadripartite cluster entanglement in the optical frequency comb," Phys. Rev. Lett. **107**, 030505 (2011).
11. M. Chen, N. C. Menicucci, and O. Pfister, "Experimental realization of multipartite entanglement of 60 modes of a quantum optical frequency comb," Phys. Rev. Lett. **112**, 120505 (2014).
12. S. Yokoyama, R. Ukai, S. C. Armstrong, C. Sornphiphatphong, T. Kaji, S. Suzuki, J. ichi Yoshikawa, H. Yonezawa, N. C. Menicucci, and A. Furusawa, "Ultra-large-scale continuous-variable cluster states multiplexed in the time domain," Nat. Photonics **7**, 982–986 (2013).
13. J. Yoshikawa, S. Yokoyama, T. Kaji, C. Sornphiphatphong, Y. Shiozawa, K. Makino, and A. Furusawa, "Generation of one-million-mode continuous-variable cluster state by unlimited time-domain multiplexing," Appl. Photonics **1(6)**, 777 (2016).

#294914 https://doi.org/10.1364/OE.25.027172
Journal © 2017 Received 21 Jun 2017; revised 9 Oct 2017; accepted 11 Oct 2017; published 23 Oct 2017

Optics EXPRESS

14. R. G. Yang, J. Zhang, S. Q. Zhai, K. Liu, J. X. Zhang, and J. R. Gao, "Generating multiplexed entanglement frequency comb in a nondegenerate optical parametric amplifier," J. Opt. Soc.Am. B **30(2)**, 314-318 (2013).
15. R. G. Yang, J. Zhang, Z. H.Zhai, S. Q. Zhai, K. Liu, and J. R. Gao, "Scheme for efficient extraction of low-frequency signal beyond the quantum limit by frequency-shift detection," Opt. Express **23**, 21323-21333 (2015).
16. R. Pooser and J. T. Jing, "Continuous-variable cluster-state generation over the optical spatial mode comb," Phys. Rev. A **90**, 043841 (2014).
17. R. G. Yang, J. J. Wang, J. Zhang, K. Liu, and J. R. Gao, "Generation of continuous-variable spatial cluster entangled states in optical mode comb," J. Opt. Soc. Am. B **33(12)**, 2424–2429 (2016).
18. K. Liu, J. Guo, C. X. Cai, J. X. Zhang, and J. R. Gao, "Direct generation of spatial quadripartite continuous variable entanglement in an optical parametric oscillator," Opt. Lett. **41**, 5178 (2016).
19. P. van Loock and A. Furusawa, "Detecting genuine multipartite continuous-variable entanglement," Phys. Rev. A **67**, 052315 (2003).
20. M. Lassen, G. Leuchs, and U. L. Andersen, "Continuous Variable Entanglement and Squeezing of Orbital Angular Momentum States," Phys. Rev. Lett. **102**, 163602 (2009).
21. L. Lopez, B. Chalopin, A. Riviére de la Souchére, C. Fabre, A. Maître, and N. Treps, "Multimode quantum properties of a self-imaging optical parametric oscillator: Squeezed vacuum and Einstein-Podolsky-Rosen-beams generation," Phys. Rev. A **80**, 043816 (2009).
22. J. A. Arnaud, "Degenerate Optical Cavities," Appl. Opt. **8**, 189–196 (1969).
23. M. Lassen, V. Delaubert, C. C. Harb, P. K. Lam, N. Treps, and H-A. Bachor, "Generation of Squeezing in Higher Order Hermite-Gaussian Modes with an Optical Parametric Amplifier," J. Eur. Opt. Soc.-Rapid **1**, 06003 (2006).
24. M. J. Collett and C. W. Gardiner, "Squeezing of intracavity and traveling-wave light fields produced in parametric amplification," Phys. Rev. A **30**, 1386-1391 (1984).
25. G. Leuchs, R. F. Dong, and D. Sych, "Triplet-like correlation symmetry of continuous variable entangled states," New J. Phys. **11**, 113040 (2009).
26. N. C. Menicucci, "Fault-tolerant measurement-based quantum computing with continuous-variable cluster states," Phys. Rev. Lett. **112**, 120504 (2014).

1. Introduction

Quantum entanglement is the most important optical resource for quantum computation [1], quantum dense coding [2] and quantum teleportation [3], which represent the foundations for construction of a quantum information network. Therefore, research on the multipartite quantum entanglement has been developed in these years. Some of generation schemes of multipartite entanglement are based on the coincident nonlinearities [4, 5]. As a special type of multipartite entanglement, the cluster states has been introduced by Raussendorf via an Ising Hamiltonian [6], which are less likely to be destroyed by local operations [7]. Additionally, the cluster states represent an effective way to realize large-scale entanglement. These states could not only speed up computation using quantum algorithms, but could also be used as a medium for quantum information transfer in quantum communication protocols. Therefore, research into the generation of cluster states has become one of the most important research fields today.

To realize usable quantum computation and quantum information processes, large-scale entanglement, i.e., multipartite entanglement between numerous subsystems, has attracted considerable focus for operation in either the frequency domain or the time domain [8, 9]. Large-scale entanglement is an interesting topic that lies at the forefront of the current research and research into such systems has begun in various laboratories. There are two common approaches that can be used to generate a large-scale cluster entangled state: one is use of a quantum optical frequency comb and the other is use of an optical spatial mode comb. In 2011, 15 quadripartite entangled cluster states were generated simultaneously over 60 consecutive Q modes in an optical frequency comb [10]. In another experiment, a cluster state in a quantum optical frequency comb with more than 60 modes that were entangled and simultaneously available was achieved [11]. Experimental demonstrations of continuous-variable (CV) cluster states have included 10,000 time-multiplexed sequentially entangled modes [12]. In 2016, one-million-mode continuous-variable cluster states by unlimited time-domain multiplexing have been generated [13]. In addition to this experimental research, we proposed a theoretical scheme to produce a multiplexed entanglement frequency comb in a nondegenerate optical parametric amplifier when operating below threshold [14] and obtained a low-frequency signal beyond the

Optics EXPRESS

quantum limit in a nondegenerate optical parametric amplifier via frequency-shift detection using frequency combs [15]. In 2014, a CV dual-rail cluster state over an optical spatial mode comb was generated in four-wave-mixing process [16]. In 2016, a scheme for generating CV spatial cluster entangled states based on optical mode combs via a large-Fresnel-number DOPO was proposed by us [17]. Other than frequency comb, spatial mode comb is a different new method for generating cluster entanglement states. Spatial freedom of light is an effective approach to scale the number of entangled states [18], which can bring new extensions and improvements. First, small interval of frequency comb depends on FSR of optical cavity, therefore it is difficult to separate them spatially in experiments. However, spatial separation of spatial modes is relative simple and efficient, by using spatial modulators. On the other hand, spatial modes are easier to detect by using Multi-quadrant detectors, CCD, etc. While the detection of the frequency comb optical field needs preparation of the local light fields with accurate frequency lines and more measurement times. In addition, such kind of spatial multipartite entanglement will be useful for future spatial multichannel quantum information application and quantum image transfer.

In this paper, we propose a new scheme to generate a large-scale CV dual-rail cluster entangled state in a specially designed self-imaging optical parametric oscillator (OPO), which can multiply the number of entangled modes. The rest of this paper is arranged as follows. In section II, our theoretical model for generating a large-scale spatial CV dual-rail cluster entangled state of Laguerre-Gaussian modes is introduced briefly and the evolution equations for the spatial modes and quadrature fluctuation are deduced. Then, the boundary conditions of the optical cavity are used to calculate the amplitude and phase quadratures of these spatial modes. In section III, the entanglement criterion that was proposed by van Loock and Furusawa for full inseparability of the optical fields [19] is used to estimate whether there is any entanglement among the CV dual-rail cluster states. Finally, a brief summary of the work is presented in section IV.

2. Theoretical model and derivation of equations

A large-scale CV dual-rail cluster state of the Laguerre-Gaussian modes is generated using a self-imaging OPO operating below threshold ($\sigma < 1$), which is pumped using two spatial Laguerre-Gaussian modes with the same frequency $2\omega_0$ and different polarizations from two-ports respectively. As is shown in Fig. 1, two periodically polarized type-zero phase-matching nonlinear crystals represented by $\chi^{(2)}$ are placed within a four-mirror ring cavity. The quasi-phase-matching crystal between flat mirror 2 and 3 (1 and 4) corresponds to zzz (yyy) parametric down-conversion (PDC), where the first letter denotes polarization of pump mode and the other two letters denote polarizations of down-converted modes. The pump fields are denoted by $\mathrm{lg}_1^{p_z}, \mathrm{lg}_{-1}^{p_y}$, which can generate spatial Laguerre-Gaussian modes $\mathrm{lg}_s^z, \mathrm{lg}_i^z$ and $\mathrm{lg}_s^y, \mathrm{lg}_i^y$ through the PDC process respectively, where $s, i = \pm1, \pm2, \pm3$ are the azimuthal mode indices, z and y represent the polarizations of the down-converted modes. Two pump fields with energy $\hbar\omega_p$ can be converted into two fields, signal and idler, with energies of $\hbar\omega_s$ and $\hbar\omega_i$ are degenerate in frequency, i.e., $\omega_s = \omega_i = \omega_0$. To generate a significant effect, the nonlinear interaction must satisfy the energy ($\hbar\omega_p$=$\hbar\omega_s + \hbar\omega_i$, $\omega_p = 2\omega_0$), momentum ($\hbar\overrightarrow{k}_p = \hbar\overrightarrow{k}_s + \hbar\overrightarrow{k}_i$) and orbit angular momentum [20]($l_p\hbar = l_s\hbar + l_i\hbar$) conservation conditions. Actually the efficiency of zzz PDC is bigger than yyy PDC for PPKTP crystals, so this four-mirror cavity of dual-port input and single-port output can be used to control waists and powers of two pump modes separately, and then the phase-matched efficiency of two crystals can be balanced. Such a cavity is a fully transverse degenerate one, which implies that all pump and down-converted modes can resonate simultaneously. From a geometrical point of view, an optical cavity is self-imaging when an arbitrary ray retraces its own path after a single round trip [21, 22]. The self-imaging ring cavity requires three lenses of focal length f_i, $i = 1, 2, 3$ and distances c_{ij} of image plane of lens i and object plane of lens j are given by $c_{1,2} = \frac{f_1 f_2}{f_3}$, $c_{1,3} = \frac{f_1 f_3}{f_2}$, $c_{2,3} = \frac{f_2 f_3}{f_1}$.

A structural diagram of a large-scale CV dual-rail cluster state is shown in Fig.

Optics EXPRESS

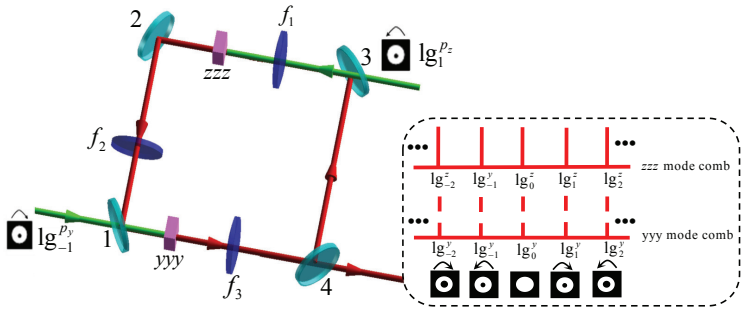

Fig. 1. Schematic of experimental setup, the green lines represent pump modes $lg_1^{p_z}$ and $lg_{-1}^{p_y}$, and the red lines represent down-converted spatial modes with different polarizations z and y, which are generated by the pump fields $lg_1^{p_z}$ and $lg_{-1}^{p_y}$. Two output mode combs are shown in the dashed box, only one part of the down-converted modes are given, and intensity profile of the down-converted modes are given below.

2. All the EPR pairs concatenate into the spatial Laguerre-Gaussian mode sequence $(\ldots lg_{-4}, lg_3, lg_{-2}, lg_1, lg_0, lg_{-1}, lg_2, lg_{-3}, lg_4 \ldots)$ shown in Fig. 2(a) that extends to the optical spatial mode comb. These spatial modes are connected by the curved arrows shown in Fig. 2(a), and comprise a large-scale CV dual-rail cluster state after passing through the single beam splitter, as shown in Fig. 2(b).

Here, the interaction Hamiltonian is:

$$\hat{H} = i\hbar \left[\sum_{s}^{1-i} \chi_m \hat{b}_1^{p_z} \hat{a}_s^{\dagger} \hat{a}_i^{\dagger} + \sum_{s}^{-1-i} \chi_m \hat{b}_{-1}^{p_y} \hat{a}_s^{\dagger} \hat{a}_i^{\dagger} \right] + H.C. \tag{1}$$

where $\chi_m, (m = 1 - 5)$ represents the effective nonlinear coupling parameter for different order parametric process, $\hat{b}_1^{p_z}$ and $\hat{b}_{-1}^{p_y}$ denote the annihilation operators for the intra-cavity pump modes, $\hat{a}_s^{\dagger}$ and $\hat{a}_i^{\dagger}$ are the creation operators of the signal and idler modes, respectively.

Here, we only consider two pump modes and twelve down-converted modes for simplicity. In the ideal case with perfect phase matching and without any detuning, the Langevin equations can be expressed as follows:

$$\begin{aligned}
\tau \dot{\hat{b}}_1^{(z)}(t) = &-\gamma_p^{(z)} \hat{b}_1^{(z)}(t) + \varepsilon_1 - \chi_1 \hat{a}_0^{(z)}(t) \hat{a}_1^{(z)}(t) - \chi_2 \hat{a}_{-1}^{(z)}(t) \hat{a}_2^{(z)}(t) - \chi_3 \hat{a}_{-2}^{(z)}(t) \hat{a}_3^{(z)}(t) \\
&+ \sqrt{2\gamma_{p_b}^{(z)}} \hat{b}_1^{in(z)}(t) + \sqrt{2\gamma_{p_c}^{(z)}} \hat{c}_{b_1}^{(z)}(t), \\
\tau \dot{\hat{b}}_{-1}^{(y)}(t) = &-\gamma_p^{(y)} \hat{b}_{-1}^{(y)}(t) + \varepsilon_{-1} - \chi_1 \hat{a}_0^{(y)}(t) \hat{a}_{-1}^{(y)}(t) - \chi_2 \hat{a}_1^{(y)}(t) \hat{a}_{-2}^{(y)}(t) - \chi_3 \hat{a}_2^{(y)}(t) \hat{a}_{-3}^{(y)}(t) \\
&+ \sqrt{2\gamma_{p_b}^{(y)}} \hat{b}_{-1}^{in(y)}(t) + \sqrt{2\gamma_{p_c}^{(y)}} \hat{c}_{b_{-1}}^{(y)}(t), \\
\tau \dot{\hat{a}}_0^{(z)}(t) = &-\gamma_0^{(z)} \hat{a}_0^{(z)}(t) + \chi_1 b_1^{(z)}(t) \hat{a}_1^{\dagger(z)}(t) + \sqrt{2\gamma_{b_0}^{(z)}} \hat{a}_0^{in(z)}(t) + \sqrt{2\gamma_{c_0}^{(z)}} \hat{c}_0^{(z)}(t), \\
\tau \dot{\hat{a}}_0^{(y)}(t) = &-\gamma_0^{(y)} \hat{a}_0^{(y)}(t) + \chi_1 b_{-1}^{(y)}(t) \hat{a}_{-1}^{\dagger(y)}(t) + \sqrt{2\gamma_{b_0}^{(y)}} \hat{a}_0^{in(y)}(t) + \sqrt{2\gamma_{c_0}^{(y)}} \hat{c}_0^{(y)}(t), \\
\tau \dot{\hat{a}}_1^{(z)}(t) = &-\gamma_1^{(z)} \hat{a}_1^{(z)}(t) + \chi_1 b_1^{(z)}(t) \hat{a}_0^{\dagger(z)}(t) + \sqrt{2\gamma_{b_1}^{(z)}} \hat{a}_1^{in(z)}(t) + \sqrt{2\gamma_{c_1}^{(z)}} \hat{c}_1^{(z)}(t), \\
\tau \dot{\hat{a}}_1^{(y)}(t) = &-\gamma_1^{(y)} \hat{a}_1^{(y)}(t) + \chi_2 b_{-1}^{(y)}(t) \hat{a}_{-2}^{\dagger(y)}(t) + \sqrt{2\gamma_{b_1}^{(y)}} \hat{a}_1^{in(y)}(t) + \sqrt{2\gamma_{c_1}^{(y)}} \hat{c}_1^{(y)}(t),
\end{aligned}$$

Optics EXPRESS

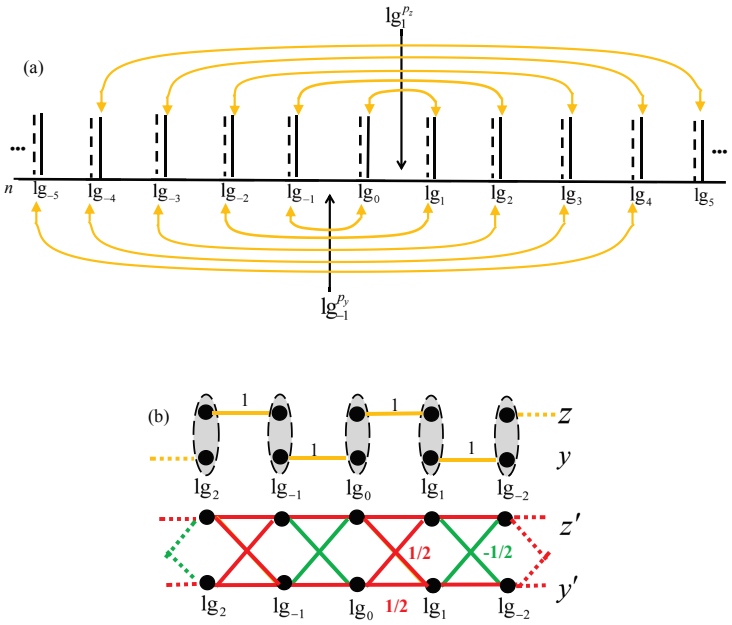

Fig. 2. (a) Structural diagram: the EPR pairs that were generated in the DOPO, the z and y modes are denoted by the red solid lines and the dashed lines, respectively. The yellow curved arrows (top) connected the zzz EPR pairs that were generated by the pump $\mathrm{lg}_1^{p_z}$ and the yellow curved arrows (bottom) connected the yyy EPR pairs that were generated by the pump $\mathrm{lg}_{-1}^{p_y}$; the vertical arrows denote the pump modes. (b) A large-scale CV dual-rail cluster entangled state: the initial EPR pairs generated by the OPO (top) turn, after passing through a single beam splitter (gray ellipses), into a CV dual-rail cluster state (bottom). Whose ±1/2 weight edges are color coded (contrary to the qubit case, weighted cluster CV states are still stabilizer states).

$$
\begin{aligned}
\tau\dot{\hat{a}}_{-1}^{(z)}(t) &= -\gamma_{-1}^{(z)}\hat{a}_{-1}^{(z)}(t) + \chi_2 b_1^{(z)}(t)\,\hat{a}_2^{\dagger(z)}(t) + \sqrt{2\gamma_{b_{-1}}^{(z)}}\,\hat{a}_{-1}^{in(z)}(t) + \sqrt{2\gamma_{c_{-1}}^{(z)}}\,\hat{c}_{-1}^{(z)}(t), \\
\tau\dot{\hat{a}}_{-1}^{(y)}(t) &= -\gamma_{-1}^{(y)}\hat{a}_{-1}^{(y)}(t) + \chi_1 b_{-1}^{(y)}(t)\,\hat{a}_0^{\dagger(y)}(t) + \sqrt{2\gamma_{b_{-1}}^{(y)}}\,\hat{a}_{-1}^{in(y)}(t) + \sqrt{2\gamma_{c_{-1}}^{(y)}}\,\hat{c}_{-1}^{(y)}(t), \\
\tau\dot{\hat{a}}_{2}^{(z)}(t) &= -\gamma_{2}^{(z)}\hat{a}_{2}^{(z)}(t) + \chi_2 b_1^{(z)}(t)\,\hat{a}_{-1}^{\dagger(z)}(t) + \sqrt{2\gamma_{b_2}^{(z)}}\,\hat{a}_{2}^{in(z)}(t) + \sqrt{2\gamma_{c_2}^{(z)}}\,\hat{c}_{2}^{(z)}(t), \\
\tau\dot{\hat{a}}_{2}^{(y)}(t) &= -\gamma_{2}^{(y)}\hat{a}_{2}^{(y)}(t) + \chi_3 b_{-1}^{(y)}(t)\,\hat{a}_{-3}^{\dagger(y)}(t) + \sqrt{2\gamma_{b_2}^{(y)}}\,\hat{a}_{2}^{in(y)}(t) + \sqrt{2\gamma_{c_2}^{(y)}}\,\hat{c}_{2}^{(y)}(t), \\
\tau\dot{\hat{a}}_{-2}^{(z)}(t) &= -\gamma_{-2}^{(z)}\hat{a}_{-2}^{(z)}(t) + \chi_3 b_1^{(z)}(t)\,\hat{a}_{3}^{\dagger(z)}(t) + \sqrt{2\gamma_{b_{-2}}^{(z)}}\,\hat{a}_{-2}^{in(z)}(t) + \sqrt{2\gamma_{c_{-2}}^{(z)}}\,\hat{c}_{-2}^{(z)}(t), \\
\tau\dot{\hat{a}}_{-2}^{(y)}(t) &= -\gamma_{-2}^{(y)}\hat{a}_{-2}^{(y)}(t) + \chi_2 b_{-1}^{(y)}(t)\,\hat{a}_{1}^{\dagger(y)}(t) + \sqrt{2\gamma_{b_{-2}}^{(y)}}\,\hat{a}_{-2}^{in(y)}(t) + \sqrt{2\gamma_{c_{-2}}^{(y)}}\,\hat{c}_{-2}^{(y)}(t), \\
\tau\dot{\hat{a}}_{3}^{(z)}(t) &= -\gamma_{3}^{(z)}\hat{a}_{3}^{(z)}(t) + \chi_3 b_1^{(z)}(t)\,\hat{a}_{-2}^{\dagger(z)}(t) + \sqrt{2\gamma_{b_3}^{(z)}}\,\hat{a}_{3}^{in(z)}(t) + \sqrt{2\gamma_{c_3}^{(z)}}\,\hat{c}_{3}^{(z)}(t), \\
\tau\dot{\hat{a}}_{-3}^{(y)}(t) &= -\gamma_{-3}^{(y)}\hat{a}_{-3}^{(y)}(t) + \chi_3 b_{-1}^{(y)}(t)\,\hat{a}_{2}^{\dagger(y)}(t) + \sqrt{2\gamma_{b_{-3}}^{(y)}}\,\hat{a}_{-3}^{in(y)}(t) + \sqrt{2\gamma_{c_{-3}}^{(y)}}\,\hat{c}_{-3}^{(y)}(t).
\end{aligned}
\tag{2}
$$

where τ is the round-trip time of the optical field inside the DOPO, χ_1, χ_2 and χ_3 are the effective nonlinear coupling parameters, $\hat{b}_1^{(z)}(\hat{b}_{-1}^{(y)})$ and $\hat{a}_i^{(z)}(\hat{a}_i^{(y)})$ are the amplitude operators of the pump modes and the down-converted modes inside the cavity, respectively. ε_1 and ε_{-1}

Optics EXPRESS

represent the pump fields that enter the cavity, and will be described classically. $\hat{b}_i^{in(z)}(\hat{b}_i^{in(y)})$ and $\hat{a}_i^{in(z)}(\hat{a}_i^{in(y)})$ denote the input amplitude operators of the pump modes and the down-converted modes, respectively. $\hat{c}_{b_i}^{(z)}(\hat{c}_{b_i}^{(y)})$ and $\hat{c}_i^{(z)}(\hat{c}_i^{(y)})$ are the excess vacuum noise operators of the pump modes and the down-converted modes, respectively.

To simplify the calculations, suppose that the two pump fields ε_1 and ε_{-1} are identical, and then the losses of the pump modes are defined as $\gamma_p = \gamma_{p_b} + \gamma_{p_c}$, where $\gamma_{p_b}, \gamma_{p_c}$ correspond to the output losses and the intra-cavity losses for the pump modes. The output coupling losses and the intra-cavity losses for the down-converted modes are the same, and are represented by $\gamma_{b_0}^{(z)} = \gamma_{b_0}^{(y)} = \gamma_{b_{\pm1}}^{(z)} = \gamma_{b_{\pm1}}^{(y)} = \gamma_{b_{\pm2}}^{(z)} = \gamma_{b_{\pm2}}^{(y)} = \gamma_{b_3}^{(z)} = \gamma_{b_{-3}}^{(y)} = \gamma_b$ and $\gamma_{c_0}^{(z)} = \gamma_{c_0}^{(y)} = \gamma_{c_{\pm1}}^{(z)} = \gamma_{c_{\pm1}}^{(y)} = \gamma_{c_{\pm2}}^{(z)} = \gamma_{c_{\pm2}}^{(y)} = \gamma_{c_3}^{(z)} = \gamma_{c_{-3}}^{(y)} = \gamma_c$, where the total loss is $\gamma = \gamma_b + \gamma_c$, and thus $\gamma_0^{(z)} = \gamma_0^{(y)} = \gamma_{\pm1}^{(z)} = \gamma_{\pm1}^{(y)} = \gamma_{\pm2}^{(z)} = \gamma_{\pm3}^{(y)} = \gamma_3^{(z)} = \gamma_{-3}^{(y)} = \gamma$.

The nonlinear coupling parameter χ_m is proportional to the overlap integral between the down-converted modes and the pump modes in the transverse plane, i.e., $\chi_m = \Gamma_{p,i,s}\chi^{(2)}$. The overlap integral is then defined as $\Gamma_{p,s,i} = \int_{-\infty}^{\infty} u_p(\vec{r})u_s(\vec{r})u_i(\vec{r})d\vec{r}$ [23], Here, $u(r)$represent the expression of the Laguerre-Gaussian modes, $u(r)$ can be simplified in the condition of p=0, the orbit angular momentum conservation, perfect phase matching and the extremely small gouy phase. We use $u_s(r)$, $u_i(r)$ as the notation for the fundamental signal and idler mode basis whose first mode has a waist of ω_0, and $u_p(r)$ for the second harmonic pump mode basis whose first mode has a waist of $\omega_0/\sqrt{2}$ [23]. The overlap coefficients are given by Table 1, the nonlinear coupling parameters are then found to be: $\chi_1 = \chi^{(2)}$, $\chi_2 = 0.707\chi^{(2)}$, and $\chi_3 = 0.433\chi^{(2)}$.

Table 1. The overlap integrals and normalizations of the down-converted modes and pump modes

p_1	$\Gamma_{1,1,0}$	$\Gamma_{1,2,-1}$	$\Gamma_{1,3,-2}$	$\Gamma_{1,4,-3}$	$\Gamma_{1,5,-4}$
p_{-1}	$\Gamma_{-1,-1,0}$	$\Gamma_{-1,-2,1}$	$\Gamma_{-1,-3,2}$	$\Gamma_{-1,-4,3}$	$\Gamma_{-1,-5,4}$
overlap integral	0.746	0.528	0.323	0.187	0.104
Normalization	1	0.707	0.433	0.250	0.140

By linearization of the operators, $\hat{b}_1^{(z)} = \beta_1^{(z)} + \delta\hat{b}_1^{(z)}$, $\hat{b}_{-1}^{(y)} = \beta_{-1}^{(y)} + \delta\hat{b}_{-1}^{(y)}$, $\hat{a}_i^{(z)} = \alpha_i^{(z)} + \delta\hat{a}_i^{(z)}$, $\hat{a}_i^{(y)} = \alpha_i^{(y)} + \delta\hat{a}_i^{(y)}$, $\hat{a}_i^{in(z)} = \delta\hat{a}_i^{in(z)}$ and $\hat{a}_i^{in(y)} = \delta\hat{a}_i^{in(y)}$, $(i = 0, \pm1, \pm2, \pm3...)$, we can obtain the steady-state equations and quantum fluctuation equations for Eq. (2). By solving the steady-state equations, the oscillation threshold ε_{th} and the pump parameter σ are expressed as $\varepsilon_{th} = \gamma\gamma_p/\chi_1$ and $\sigma = \varepsilon/\varepsilon_{th}$, respectively. The steady-state solution is given by $\beta_{\pm1}^{(z/y)} = \varepsilon/\gamma$ and $\alpha_0^{(z)} = \alpha_0^{(y)} = \alpha_{\pm1}^{(z)} = \alpha_{\pm1}^{(y)} = \alpha_{\pm2}^{(z)} = \alpha_{\pm2}^{(y)} = \alpha_3^{(z)} = \alpha_{-3}^{(y)} = 0$. The quantum fluctuation equations perform a Fourier transformation, we can then obtain the fluctuation dynamics equations. By applying the definitions of the amplitude and phase quadratures, i.e., $\hat{X} = \hat{a} + \hat{a}^\dagger$ and $\hat{Y} = (\hat{a} - \hat{a}^\dagger)/i$, the amplitude quadratures of the down-converted spatial modes can then be expressed as follows:

Optics EXPRESS

$$M_x \begin{pmatrix} \delta\hat{Q}_0^{(z)}(\omega) \\ \delta\hat{Q}_1^{(z)}(\omega) \\ \delta\hat{Q}_{-1}^{(z)}(\omega) \\ \delta\hat{Q}_2^{(z)}(\omega) \\ \delta\hat{Q}_{-2}^{(z)}(\omega) \\ \delta\hat{Q}_3^{(z)}(\omega) \end{pmatrix} = \sqrt{2\gamma_b} \begin{pmatrix} \delta\hat{Q}_0^{in(z)}(\omega) \\ \delta\hat{Q}_1^{in(z)}(\omega) \\ \delta\hat{Q}_{-1}^{in(z)}(\omega) \\ \delta\hat{Q}_2^{in(z)}(\omega) \\ \delta\hat{Q}_{-2}^{in(z)}(\omega) \\ \delta\hat{Q}_3^{in(z)}(\omega) \end{pmatrix} + \sqrt{2\gamma_c} \begin{pmatrix} \delta\hat{Q}_{c_0}^{(z)}(\omega) \\ \delta\hat{Q}_{c_1}^{(z)}(\omega) \\ \delta\hat{Q}_{c_{-1}}^{(z)}(\omega) \\ \delta\hat{Q}_{c_2}^{(z)}(\omega) \\ \delta\hat{Q}_{c_{-2}}^{(z)}(\omega) \\ \delta\hat{Q}_{c_3}^{(z)}(\omega) \end{pmatrix},$$

$$M_y \begin{pmatrix} \delta\hat{Q}_0^{(y)}(\omega) \\ \delta\hat{Q}_1^{(y)}(\omega) \\ \delta\hat{Q}_{-1}^{(y)}(\omega) \\ \delta\hat{Q}_2^{(y)}(\omega) \\ \delta\hat{Q}_{-2}^{(y)}(\omega) \\ \delta\hat{Q}_3^{(y)}(\omega) \end{pmatrix} = \sqrt{2\gamma_b} \begin{pmatrix} \delta\hat{Q}_0^{in(y)}(\omega) \\ \delta\hat{Q}_1^{in(y)}(\omega) \\ \delta\hat{Q}_{-1}^{in(y)}(\omega) \\ \delta\hat{Q}_2^{in(y)}(\omega) \\ \delta\hat{Q}_{-2}^{in(y)}(\omega) \\ \delta\hat{Q}_3^{in(y)}(\omega) \end{pmatrix} + \sqrt{2\gamma_c} \begin{pmatrix} \delta\hat{Q}_{c_0}^{(y)}(\omega) \\ \delta\hat{Q}_{c_1}^{(y)}(\omega) \\ \delta\hat{Q}_{c_{-1}}^{(y)}(\omega) \\ \delta\hat{Q}_{c_2}^{(y)}(\omega) \\ \delta\hat{Q}_{c_{-2}}^{(y)}(\omega) \\ \delta\hat{Q}_{c_3}^{(y)}(\omega) \end{pmatrix}. \tag{3}$$

Here,

$$M_x = \begin{pmatrix} i\omega\tau+\gamma & -\chi_1\beta_1^{(z)} & 0 & 0 & 0 & 0 \\ -\chi_1\beta_1^{(z)} & i\omega\tau+\gamma & 0 & 0 & 0 & 0 \\ 0 & 0 & i\omega\tau+\gamma & -\chi_2\beta_2^{(z)} & 0 & 0 \\ 0 & 0 & -\chi_2\beta_2^{(z)} & i\omega\tau+\gamma & 0 & 0 \\ 0 & 0 & 0 & 0 & i\omega\tau+\gamma & -\chi_3\beta_3^{(z)} \\ 0 & 0 & 0 & 0 & -\chi_3\beta_3^{(z)} & i\omega\tau+\gamma \end{pmatrix},$$

$$M_y = \begin{pmatrix} i\omega\tau+\gamma & 0 & -\chi_1\beta_{-1}^{(y)} & 0 & 0 & 0 \\ 0 & i\omega\tau+\gamma & 0 & 0 & -\chi_2\beta_{-2}^{(y)} & 0 \\ -\chi_1\beta_{-1}^{(y)} & 0 & i\omega\tau+\gamma & 0 & 0 & 0 \\ 0 & 0 & 0 & i\omega\tau+\gamma & 0 & -\chi_3\beta_{-3}^{(y)} \\ 0 & -\chi_2\beta_{-2}^{(y)} & 0 & 0 & i\omega\tau+\gamma & 0 \\ 0 & 0 & 0 & -\chi_3\beta_{-3}^{(y)} & 0 & i\omega\tau+\gamma \end{pmatrix}. \tag{4}$$

The matrix forms of the phase quadratures can be obtained in a similar manner. Using the boundary conditions [24] of $\delta\hat{Q}_i^{out} = \sqrt{2\gamma_{bi}}\delta\hat{Q}_i - \delta\hat{Q}_i^{in}$ and $\delta\hat{P}_i^{out} = \sqrt{2\gamma_{bi}}\delta\hat{P}_i - \delta\hat{P}_i^{in}$, $(i = 0, \pm1, \pm2, \pm3\ldots)$, we can then calculate the amplitude and phase quadratures for the different polarization modes. The two different polarization modes z and y turn into a CV dual-rail cluster entangled state after passing through a single 50/50 beam splitter with a relative phase of $\pi/2$ [25]. The resulting output modes (after the beam splitter) are then labeled z' and y', respectively. The beam splitter transformation is given by $\hat{a}^{(z')} = \frac{1}{\sqrt{2}}\left(\hat{a}^{(z)} + i\hat{a}^{(y)}\right)$ and $\hat{a}^{(y')} = \frac{1}{\sqrt{2}}\left(\hat{a}^{(z)} - i\hat{a}^{(y)}\right)$, and thus the amplitude and phase quadratures of the output modes are as follows: $\hat{Q}_{\mathrm{i}}^{(z')} = \frac{1}{\sqrt{2}}\left(\hat{Q}_i^{(z)} - \hat{P}_i^{(y)}\right)$, $\hat{P}_i^{(z')} = \frac{1}{\sqrt{2}}\left(\hat{P}_i^{(z)} + \hat{Q}_i^{(y)}\right)$, $\hat{Q}_{\mathrm{i}}^{(y')} = \frac{1}{\sqrt{2}}\left(\hat{Q}_i^{(z)} + \hat{P}_i^{(y)}\right)$, $\hat{P}_i^{(y')} = \frac{1}{\sqrt{2}}\left(\hat{P}_i^{(z)} - \hat{Q}_i^{(y)}\right)$. Based on Eq. (3), the amplitude and phase quadratures of the modes $\mathrm{lg}_0^{(z')}$, $\mathrm{lg}_0^{(y')}$, $\mathrm{lg}_{\pm1}^{(z')}$, $\mathrm{lg}_{\pm1}^{(y')}$ ... can now be obtained.

3. Sufficient conditions for overall inseparability

The quantum entanglements of the CV dual-rail cluster states are characterized via the correlations of their amplitude and phase quadratures. Based on the entanglement criterion proposed by van

Optics EXPRESS

Loock and Furusawa for the inseparability [13, 19], we consider the criterion for all possible separable bipartitions in our set of output modes and obtain sufficient conditions for overall inseparability:

$$Q_{s.i} = \left\langle \left(\left(\hat{Q}_s^{z'} + \hat{Q}_s^{y'} \right) - \left(\hat{Q}_i^{z'} + \hat{Q}_i^{y'} \right) \right)^2 \right\rangle < 1/2, \tag{5}$$

$$P_{s.i} = \left\langle \left(\left(\hat{P}_s^{z'} + \hat{P}_s^{y'} \right) + \left(\hat{P}_i^{z'} + \hat{P}_i^{y'} \right) \right)^2 \right\rangle < 1/2, \tag{6}$$

$$Q_{s.i} = \left\langle \left(\left(\hat{Q}_i^{z'} - \hat{Q}_i^{y'} \right) + \left(\hat{Q}_s^{z'} - \hat{Q}_s^{y'} \right) \right)^2 \right\rangle < 1/2, \tag{7}$$

$$P_{s.i} = \left\langle \left(\left(\hat{P}_i^{z'} - \hat{P}_i^{y'} \right) - \left(\hat{P}_s^{z'} - \hat{P}_s^{y'} \right) \right)^2 \right\rangle < 1/2. \tag{8}$$

$s + i = 1$ corresponds to Eqs. (5) and (6), whereas $s + i = -1$ corresponds to Eqs. (7) and (8), and 1/2 is the shot-noise limit. The quantum entanglements of the spatial CV dual-rail cluster states are vividly illustrated in Fig. 3. The quantum entanglement of Eqs. (5) to (8) can be measured via two-tone balanced homodyne detection using spatially tailored local oscillator (LO) modes at ω_0, where the quadrature combinations can be fed into a spectrum analyzer that is used to display the noise power in experiment. Calculations show that the results of Eqs. (5) and (6) [and those of Eqs. (7) and (8)] are identical.

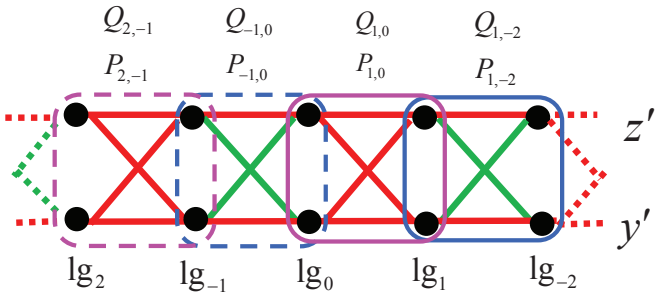

Fig. 3. Visualization of quantum entanglements of Eqs. (5) to (8) in the CV dual-rail cluster states shown in Fig. 2(b).

Figure 4 shows the quantum entanglement of $Q_{i,s}$ $(P_{i,s})$ $(i, s = 0, 1, i, s = 0, -1, i, s = -1, 2, i, s = 1, -2, i, s = -2, 3, i, s = 2, -3, i, s = -3, 4, i, s = 3, -4, i, s = -4, 5, i, s = 4, -5)$ versus the normalized analyzing frequency $\Omega = \omega\tau/\gamma$. The entanglement decreases gradually with the normalized analyzing frequency. It satisfies the sufficient conditions for overall inseparability over a wide range of normalized analyzing frequency when we select the proper pump parameter. As is shown, the trends of all curves are similar.

Figure 5 shows the quantum entanglement of $Q_{i,s}$ $(P_{i,s})$ $(i, s = 0, 1, i, s = 0, -1, i, s = -1, 2, i, s = 1, -2, i, s = -2, 3, i, s = 2, -3, i, s = -3, 4, i, s = 3, -4, i, s = -4, 5, i, s = 4, -5)$ versus the pump parameter $\sigma = \varepsilon/\varepsilon_{th}$ (which has been normalized with respect to the pump threshold). The entanglements grow with increasing pump parameter and the largest entanglement can be obtained near the threshold. This satisfies the sufficient conditions for overall inseparability when the DOPO is operating below threshold ($\sigma < 1$).

As clearly shown in Figs. 4 and 5, the first-order quantum entanglement satisfy the condition $Q_{0,1} = Q_{0,-1}$ because the spatial mode EPR pairs $\mathrm{lg}_0^{(z)} \sim \mathrm{lg}_1^{(z)}$ and $\mathrm{lg}_0^{(y)} \sim \mathrm{lg}_{-1}^{(y)}$ correspond to the same nonlinear coupling parameter χ_1, and similarly, $Q_{-1,2} = Q_{1,-2}$, $Q_{-2,3} = Q_{2,-3}$,

Optics EXPRESS

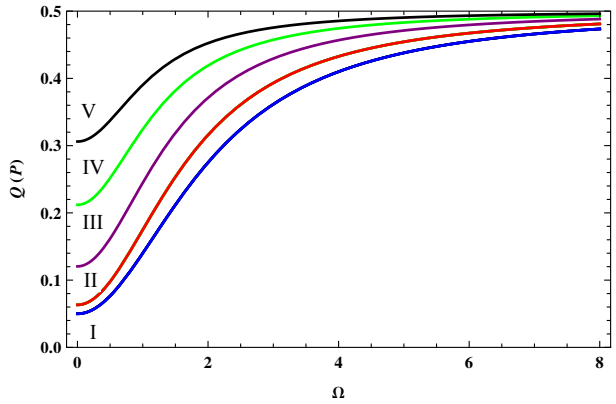

Fig. 4. Quantum entanglement versus normalized frequency $\Omega = \omega\tau/\gamma$ with $\gamma_p = 0.025$, $\gamma = 0.02$, $\gamma_b = 0.018$, $\gamma_c = 0.002$, $\chi_1 = \chi^{(2)}$, $\chi_2 = 0.707\chi^{(2)}$, $\chi_3 = 0.433\chi^{(2)}$, $\chi_4 = 0.250\chi^{(2)}$, $\chi_5 = 0.140\chi^{(2)}$ and $\sigma = 0.8$. (I): $Q_{1,0} = Q_{0,-1} = P_{1,0} = P_{0,-1}$, blue line; (II): $Q_{2,-1} = Q_{1,-2} = P_{2,-1} = P_{1,-2}$, red line; (III): $Q_{3,-2} = Q_{2,-3} = P_{3,-2} = P_{2,-3}$, purple line; (IV): $Q_{4,-3} = Q_{3,-4} = P_{4,-3} = P_{3,-4}$, green line; (V): $Q_{5,-4} = Q_{4,-5} = P_{5,-4} = P_{4,-5}$, black line.

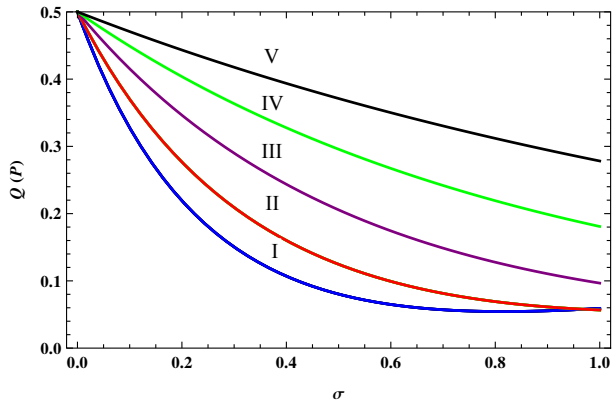

Fig. 5. Quantum entanglement versus pump parameter $\sigma = \varepsilon/\varepsilon_{th}$ with $\gamma_p = 0.025$, $\gamma = 0.02$, $\gamma_b = 0.018$, $\gamma_c = 0.002$, $\chi_1 = \chi^{(2)}$, $\chi_2 = 0.707\chi^{(2)}$, $\chi_3 = 0.433\chi^{(2)}$, $\chi_4 = 0.250\chi^{(2)}$, $\chi_5 = 0.140\chi^{(2)}$ and $\Omega = 0.2$. (I): $Q_{1,0} = Q_{0,-1} = P_{1,0} = P_{0,-1}$, blue line; (II): $Q_{2,-1} = Q_{1,-2} = P_{2,-1} = P_{1,-2}$, red line; (III): $Q_{3,-2} = Q_{2,-3} = P_{3,-2} = P_{2,-3}$, purple line; (IV): $Q_{4,-3} = Q_{3,-4} = P_{4,-3} = P_{3,-4}$, green line; (V): $Q_{5,-4} = Q_{4,-5} = P_{5,-4} = P_{4,-5}$, black line.

$Q_{-3,4} = Q_{3,-4}$, $Q_{-4,5} = Q_{4,-5}$. Additionally, for the relation of nonlinear coupling parameters: $\chi_1 > \chi_2 > \chi_3 > \chi_4 > \chi_5$, with the nonlinear coupling parameter decreases gradually, the quantum entanglement decreases. Therefore the quantum entanglements of $Q_{0,1}$ and $Q_{0,-1}$ are the largest, and the quantum entanglements of $Q_{-4,5}$ and $Q_{4,-5}$ are the smallest. We confirm that at least 20 entangled modes can be generated by considering periodicity of entanglement. And the squeezing degree of the noise correlation between the different modes is expected to be detected in experiments, and the squeezing at zero frequency can reach 10.1dB, 9.1dB, 6.2dB, 3.7dB, 2.2dB, respectively.

It should be noted that the weights here are 1/2 and -1/2, because all modes passing through a single 50/50 beam splitter. Under this condition, the entanglement criterion is satisfied indeed,

Optics EXPRESS

even though it is not optimum.

4. Conclusions

In this work, we proposed a new scheme to generate a large-scale CV dual-rail cluster state of Laguerre-Gaussian modes based on a spatial mode comb in a self-imaging OPO when operating below threshold; the scheme can be distinguished from other schemes of the frequency domain and the time domain. Their constant entanglement versus the normalized analyzing frequency and the pump parameter can be observed under sufficient conditions for full inseparability. The dual-rail cluster states of the 20 fully inseparable light modes can be generated using strong pump power, a high $\chi^{(2)}$ and a higher $\Gamma_{p,i,s}$. If we can achieve the following conditions, e.g., perfect mode-matching, alignment of the interactional modes and special transverse pump structure, a larger parametric interaction and a larger-scale entanglement (i.e., more than 20 spatial modes) will be realized. This scheme can pave a new way to generate large-scale CV cluster entangled states using spatial mode combs, which can then be applied extensively in the fields of the quantum computing, and the relevance of continuous variables for cluster states is also important to universal quantum computing because of potential for scalability and a fault tolerance [11, 26].

Funding

National Natural Science Foundation of China (NSFC) (11504218, 61108003, 91536222, 61405108); Natural Science Foundation of Shanxi Province, China (2013021005-2); National Key Research and Development Plan (2016YFA0301404).